Received: April 27, 2022 | Accepted: May 20, 2022 | Web Released: July 21, 2022 CL-220215

Free Energy and Solvation Structure Analysis for Adsorption of Aromatic Molecules at Pt(111)/Water Interface by 3D-RISM Theory

Akihiko Takamatsu,[1] Masahiro Higashi,[1,2] and Hirofumi Sato*[1,2,3]
[1]*Department of Molecular Engineering, Kyoto University, Nishikyo-ku, Kyoto 615-8510, Japan*
[2]*Elements Strategy Initiative for Catalysts and Batteries (ESICB), Kyoto University, Nishikyo-ku, Kyoto 615-8520, Japan*
[3]*Fukui Institute for Fundamental Chemistry, Kyoto University, Sakyo-ku, Kyoto 606-8103, Japan*

E-mail: hirofumi@moleng.kyoto-u.ac.jp

The free energy change of aromatic molecules adsorbed at a Pt(111)/water interface was analyzed using the three-dimensional reference interaction site model (3D-RISM) theory with density functional theory (DFT), compared with the reported experimental data. The changes in the solvation structure induced by molecular adsorption were discussed.

Keywords: Chemisorption | 3D-RISM | Solid-liquid interface

The adsorption free energy at solid-liquid interfaces ($\Delta G^{\mathrm{ad(liq)}}$) is fundamental to understanding the physical chemistry at interfaces. But it has been difficult to observe $\Delta G^{\mathrm{ad(liq)}}$ experimentally, and the effect of water, the primary solvent, has not been fully clarified.[1] However, progress in observation techniques using electrochemical methods at the Pt(111)/water interface has been reported.[2–6] The experimental results have not only been analyzed by a simple bond-additivity model[3,7] based on a thermodynamic cycle relationship, but also have promoted the development of a new theoretical model.[8–10]

The theory for evaluating $\Delta G^{\mathrm{ad(liq)}}$ has difficulties in dealing with solvent ordering in the vicinity of an interface. Both strong adsorption of solvent molecules by solid surfaces and thermal fluctuations in structure must be considered. The implicit solvent model, such as the polarizable continuum model (PCM),[11,12] in which a homogeneous dielectric media represents solvent molecules, is the most commonly used with the advantage of the relatively small computational cost. But care must be taken in cavity parameterization to reproduce experimental tendencies.[4,10] Another option is the free energy perturbation/molecular dynamics method (FEP/MD).[13] Although it requires extensive configurational sampling of solvent molecules and adsorbates, it reproduces qualitative trends of $\Delta G^{\mathrm{ad(liq)}}$ when combined with DFT.[8]

Alternatively, a statistical mechanical theory, e.g. the integral equation of molecular liquids like the reference interaction site model (RISM), is applied[14–17] and developed[18] for solid-liquid interfacial systems. It is free from so-called "sampling error", enabling us to obtain an adequate statistical ensemble of solvent configuration within a reasonable computational load due to its analytical nature. RISM and its 3D version (3D-RISM) can analyze the solvation structure in complex environments.[19,20]

In this study, the adsorption of aromatic molecules at the Pt(111)/water interface is computed with the 3D-RISM method[16,17] and DFT. The utilization of 3D-RISM and its combination with DFT allows us to calculate the free energies of adsorption at the solid/liquid interface, including the electronic structure change, and compare them with the experimental data of aromatic molecules for the first time.

The platinum (111) surface is modeled as a 4-layered slab with two bottom layers fixed to its bulk geometry. The adsorption configuration of benzene and phenol was in accordance with the most stable one shown in previous DFT calculations[21,22] where aromatic molecules are adsorbed at the bridge site with the axis of the aromatic ring rotated by 30° for the line of surface Pt atoms (See Figure S1). For different adsorption rates of 1/16 and 1/36, the surface area of the slab model was varied as 4×4 and 6×6, respectively. The absorption rate is defined as the number of aromatic molecules adsorbed relative to the number of surface Pt atoms per unit cell. *k*-point sampling was performed to ensure that the adsorption energy of molecules was sufficiently converged for each slab model. The vacuum layer was set as 15 Å. Molecules of benzene, phenol and water are computed in a cubic box of a length 20 Å with gamma point sampling of *k*-points.

The DFT calculations were carried out with the Vienna Ab initio Simulation Package (VASP).[23,24] The electronic structure was described within generalized gradient approximation using the exchange and correlation functional parametrized by Perdew, Burke, and Ernzerhof (PBE),[25] using projector augmented wave (PAW) method.[26] The dispersion force correction was described by dDsC approach.[27] The cut-off energy for the plane-wave basis set was set to 400 eV. Dipole correction[28] for the *z*-direction was applied to avoid periodic summation of the induced dipole. The *k*-point mesh was sampled with $3 \times 3 \times 1$ meshes using the Monkhorst-Pack scheme.[29] The unfixed geometries were optimized by DFT with van der Waals force correction until reaching the threshold for a residual force of 0.02 eV/Å and total energy difference of 0.01 eV, respectively. Atomic charges were determined by the CM5 method[30] using Chargemol program.[31,32] The values of each atomic charge were multiplied by 1.27, taking into account the polarization effect in the liquid phase.[33] These procedures for model construction are written in a recent paper[8] reporting FEP/MD simulation for the same system.

The 3D-RISM theory was utilized to calculate the solvation. The equation[16,17] is written as

$$h_\gamma(\mathbf{r}) = \sum_\alpha \int d\mathbf{r}' c_\alpha(\mathbf{r}-\mathbf{r}')\chi_{\alpha\gamma}(r') \qquad (1)$$

where $c_\alpha(\mathbf{r})$, $h_\gamma(\mathbf{r})$, and $\chi_{\alpha\gamma}(\mathrm{r})$ are the direct correlation function, total correlation function, and site–site susceptibility function, respectively. $h_\gamma(\mathbf{r})$ is related with 3D site distribution function $g_\gamma(\mathbf{r})$ by $h_\gamma(\mathbf{r}) = g_\gamma(\mathbf{r}) - 1$. The α and γ stand for the index of atomic site in solute and solvent, respectively. Equation (1) is closed by the following Kovalenko-Hirarta (KH) closure relation[17]

$$g_\gamma(\mathbf{r}) = \begin{cases} \exp(-u_\gamma(\mathbf{r})/(k_\mathrm{B}T) + h_\gamma(\mathbf{r}) - c_\gamma(\mathbf{r})) & \text{for } g_\gamma(\mathbf{r}) \le 1 \\ 1 - u_\gamma(\mathbf{r})/(k_\mathrm{B}T) + h_\gamma(\mathbf{r}) - c_\gamma(\mathbf{r}) & \text{for } g_\gamma(\mathbf{r}) > 1 \end{cases} \quad (2)$$

where $u_\gamma(\mathbf{r})$ is the 3D interaction potential between the whole solute and solvent site γ specified by a molecular force field, and $k_\mathrm{B}T$ is the Boltzmann constant times the solution temperature. The site-site susceptibility of solvent is composed of intramolecular and intermolecular terms,

$$\chi_{\alpha\gamma}(r) = \omega_{\alpha\gamma}(r) + \rho_\alpha h_{\alpha\gamma}(r) \quad (3)$$

where the intermolecular correlation function $\omega_{\alpha\gamma}(r) = \delta_{\alpha\gamma}\delta(r) + (1 - \delta_{\alpha\gamma})\delta(r - l_{\alpha\gamma})/4\pi l_{\alpha\gamma}{}^2$ represents the geometry of solvent molecule with site–site separations $l_{\alpha\gamma}$. ρ_α is density of bulk solvent. Beforehand of the 3D-RISM calculation, $h_{\alpha\gamma}(\mathbf{r})$ was obtained from the dielectrically consistent RISM theory[34] (DRISM) coupled with the KH closure. Equations (1) and (2) are solved iteratively by using the modified direct inversion in the iterative subspace (MDIIS) theory.

Solvation free energy was calculated by the following equation[16,17]

$$\mu^{\mathrm{KH}}_{\mathrm{solv}} = k_\mathrm{B}T \sum_\gamma \rho_\gamma \int \mathrm{d}\mathbf{r} \left[\frac{1}{2} h_\gamma^2(\mathbf{r}) \Theta(-h_\gamma(\mathbf{r})) - c_\gamma(\mathbf{r}) - \frac{1}{2} h_\gamma(\mathbf{r}) c_\gamma(\mathbf{r}) \right] \quad (4)$$

where $\Theta(x)$ is the Heaviside step function.

The interaction potential $u_\gamma(\mathbf{r})$ is composed of 12-6 Lennard-Jones and Coulomb forms

$$u_\gamma(\mathbf{r}) = u^{\mathrm{LJ}}_\gamma(\mathbf{r}) + u^{\mathrm{ele.}}_\gamma(\mathbf{r}) \quad (5)$$

$$u^{\mathrm{LJ}}_\gamma(\mathbf{r}) = \sum_\alpha 4\varepsilon_{\alpha\gamma} \left[\left(\frac{\sigma_{\alpha\gamma}}{|\mathbf{r} - \mathbf{R}_\alpha|} \right)^{12} - \left(\frac{\sigma_{\alpha\gamma}}{|\mathbf{r} - \mathbf{R}_\alpha|} \right)^{6} \right] \quad (6)$$

$$u^{\mathrm{ele.}}_\gamma(\mathbf{r}) = q_\gamma \left[\sum_\alpha \frac{q_\alpha}{|\mathbf{r} - \mathbf{R}_\alpha|} \right] \quad (7)$$

where q_α and q_γ are the partial atomic charges of solute and solvent interacting sites, $\sigma_{\alpha\gamma}$, $\varepsilon_{\alpha\gamma}$ are the Lennard-Jones parameters determined by Lolentz-Berthelot rule, and $|\mathbf{r} - \mathbf{R}_\alpha|$ is the distance between interacting sites of solute and solvent. The parameters for aromatic molecules and surface Pt atoms were described by universal force field (UFF)[35] and those fitted by Heinz *et al.*[36] to reproduce the solid-liquid interfacial free energy, respectively (See Table 1). The lattice size and the number of grid points used for 3D-RISM calculation are given in supporting information.

Figure 1 illustrates the adsorption process considered in this study. The Gibbs free energy change associated with adsorption in the solution phases, $\Delta G^{\mathrm{ad(liq)}}$ is as follows,

Table 1. Lennard-Jones parameters and atomic charges used in the 3D-RISM equation. For specific charge values, see supporting information.

Element	ε/kcal mol^{-1}	σ/Å	Charge
Pt	7.800	2.534	DFT(CM5)
C	0.105	3.431	DFT(CM5)
O	0.060	3.118	DFT(CM5)
H	0.044	2.571	DFT(CM5)
O (H_2O)	0.155	3.166	SPC
H (H_2O)	0.056	1.000	SPC

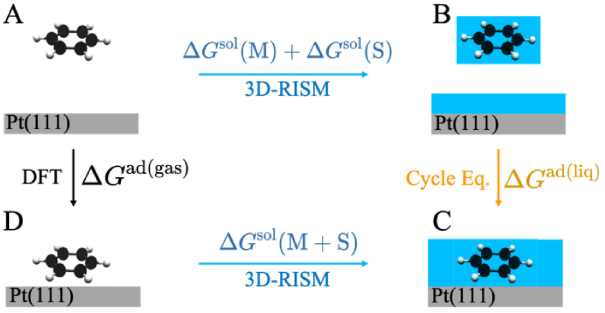

Figure 1. Free energy of the adsorption process at the solid-liquid interface. M, S, and M + S are the molecule, surface, and entire adsorption system, respectively.

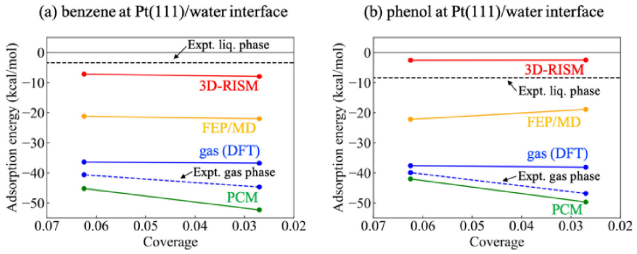

Figure 2. Adsorption free energy for (a) benzene and (b) phenol adsorption system. PCM and FEP/MD values are taken from ref 8. To note that, the adsorption energy of experimental and DFT at gas phase are enthalpy[38,39] and free energy calculated by eq. (9), respectively.

$$\Delta G^{\mathrm{ad(liq)}} = \Delta G^{\mathrm{ad(gas)}} + \Delta G^{\mathrm{sol}}(\mathrm{M+S}) - (\Delta G^{\mathrm{sol}}(\mathrm{M}) + \Delta G^{\mathrm{sol}}(\mathrm{S})) \quad (8)$$

where $\Delta G^{\mathrm{ad(gas)}}$ is the adsorption free energy change in the gas phase. $\Delta G^{\mathrm{ad(gas)}}$ is evaluated as

$$\Delta G^{\mathrm{ad(gas)}} = \Delta E^{\mathrm{ad(gas)}} - T\Delta S^{\mathrm{ad(gas)}} \quad (9)$$

where $\Delta E^{\mathrm{ad(gas)}}$ is a difference of internal energy change $\Delta E^{\mathrm{ad(gas)}} = E(\mathrm{M+S}) - (E(\mathrm{M}) + E(\mathrm{S}))$ by DFT and $\Delta S^{\mathrm{ad(gas)}}$ is evaluated by empirical formula.[37] It is noted that zero-point energy changes were neglected because they were smaller than 1.0 kcal/mol. The solvation free energies of the molecule, surface, and entire system transfer from the gas phase to the solution phase are denoted by $\Delta G^{\mathrm{sol}}(\mathrm{X})$ (X = M, S, M + S), where all of them are evaluated with 3D-RISM using eq. (4).

Figure 2 shows the adsorption free energy change for (a) benzene and (b) phenol ($\Delta G^{\mathrm{ad(gas)}}$ and $\Delta G^{\mathrm{ad(liq)}}$) as a function of the "adsorption rate θ" at the Pt(111)/water interface. That is the number of aromatic molecules relative to the surface Pt atoms per unit cell. Since one molecule is adsorbed in each cell, a small value corresponds to a calculation using a large cell. The experimental reports are −3.4 kcal/mol and −8.4 kcal/mol for benzene and phenol molecule.[3] In contrast, the adsorption energies measured in the gas phase are about −30 to −40 kcal/mol for both benzene and phenol.[38,39]

The present results denoted with 3D-RISM are relatively independent of the cell size and improve the agreement with the experiments. It should be noted that $T\Delta S^{\mathrm{ad(gas)}}$ is not included in the FEP/MD. For the benzene system, $\Delta G^{\mathrm{ad(liq)}}$ is −7.9 and

-7.1 kcal/mol for $\theta = 0.027$ and 0.0625, respectively, close to the measured -3.4 kcal/mol[3]. A noticeable difference of the present method compared to PCM is the treatment of specific solute-solvent interactions such as hydrogen bonding. Due to the analytical nature of the 3D-RISM, the present method is free from the difficulty in the generation of the statistical ensemble, which could be complicated in the heterogenous system. For the phenol system, the present result (-2.5 and -2.6 kcal/mol for $\theta = 0.027$ and 0.0625, respectively) shows a reasonable agreement with the experiments, but the stabilization by the adsorption is slightly underestimated.

The adsorption of an aromatic molecule at the solid/water interface is less stabilized than that at the solid/air interface. The difference is explained in that water molecules adsorbed on the metal surface must be kicked out for the aromatic molecules to absorb.[2–4] Therefore, the evaluation of $\Delta G^{\mathrm{ad(liq)}}$ requires an accurate description of the thermodynamic quantities of the desolvation process. The solvation free energy ΔG^{sol} of the Pt(111) surface per surface Pt atom has been estimated[10] to be between -1.04 and -1.71 kcal mol^{-1} atom^{-1}. In the present 3D-RISM, it is estimated to be -3.9 kcal mol^{-1} atom^{-1} (For the details, please see supporting information), which is in better agreement than that calculated with PCM to determine the cavity on the isodensity surface of electron (-0.057 kcal mol^{-1} atom^{-1})[9] and as accurate as that calculated with FEP/MD (-5.2 kcal mol^{-1} atom^{-1}).[8] It has been pointed out that the commonly used PCM[12] employs the same cavity parameterization for metal surfaces and organic molecules, resulting in a decreased accuracy.[9] On the other hand, 3D-RISM is considered more accurate because it explicitly considers the interactions between solvent and metal surface or adsorbate.

The solvation structure around the absorbing molecule is another essential piece of information. For homogeneous solvent systems, the molecular details have been investigated to date. For example, phenol in aqueous media forms σ-type hydrogen bonds with OH groups and forms π-type hydrogen bonds derived from π electrons of benzene rings.[40,41] On the other hand, unique solvation structures near the solid surface are reported by experimental and theoretical studies.[42–44] A RISM study reports a unique orientation of water molecules near a solid surface.[45] An MD simulation on the solvation structure around adsorbed molecules at a Cu(111) surface reported the estimation of the number of hydrogen bonds around the adsorbed molecules from snapshots of the local solvent configuration.[46]

Figure 3(a) and (b) show the spatial distribution function of water on the Pt(111) surface obtained by the 3D-RISM equation, with the origin of the z-axis at the center of the topmost Pt atom. For the oxygen (a), $g_{\mathrm{O}}(\mathbf{r})$, there are no water molecules in $z = 0$ to 2 Å region, because of the exclusion potential of Pt atoms. Around $z = 2.5$ Å, one can see the high value (more than 5.5) region colored with red, corresponding to the bridge and hollow sites. The second peak is found around $z = 5.5$ Å depicted with the orange color, and the oscillatory behavior gradually converges to the uniform distribution. Figure 3(c) plots the distribution perpendicular to the surface from top, bridge, and hollow sites. The average of all these is also shown. As clearly seen, the first peaks are high for the bridge and hollow sites. In contrast, the curves are almost coincident beyond the second peak, indicating that the effect from the surface becomes sufficiently weakened and the distribution of water becomes

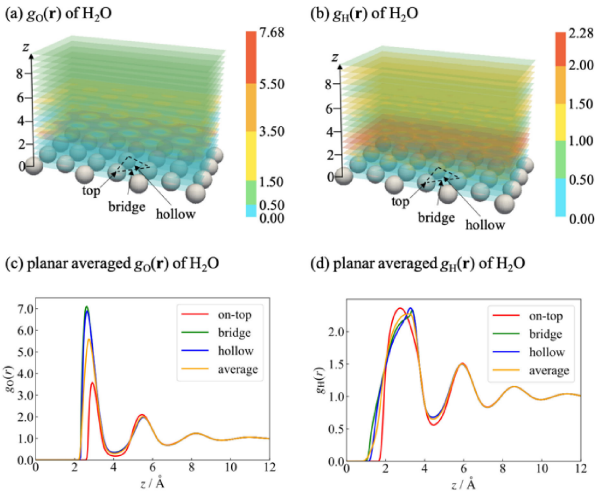

Figure 3. (a) and (b) are the spatial distribution functions $g_\gamma(\mathbf{r})$ of water near a Pt(111) surface. The contour maps of $g_\gamma(\mathbf{r})$ are shown in cross sections every 0.5 Å along the z-axis. (c) and (d) are the distribution functions along the z-axis and are calculated by averaging $g_\gamma(\mathbf{r})$ in the xy-plane and perpendicular to the surface from on-top, bridge, and hollow sites.

uniform. Figure 3(b) shows the spatial distribution of hydrogen sites $g_{\mathrm{H}}(\mathbf{r})$. Please note that the color scale is smaller than that for oxygen, and maximum value is less than 2.5. Unlike the $g_{\mathrm{O}}(\mathbf{r})$, the color is generally blurred and there are no specific adsorption sites. The highest distribution is found from $z = 2.5$ to 3.5 Å (shown in orange). On looking at the averaged distributions shown in Figure 3(d), the rises of the peaks are much shorter for hollow and bridge sites than for the top, while the location of the first peak is closest for the top site. The first peaks are not sharp, which may be attributed to a combination of several configurations of solvation. Similar to the oxygen, the curves for the entire site are almost identical beyond the second peak. Comparing $g_{\mathrm{O}}(\mathbf{r})$ and $g_{\mathrm{H}}(\mathbf{r})$, the positions of the peaks are almost the same, and the width of the peak for the hydrogen is wider (see Figure 3(c) and Figure 3(d)). This suggests that the interaction between the surface and solvent molecule is not so strong, and water molecules in the vicinity of the surface are oriented in various ways.

Let us dissolve the aromatic molecule to see how the liquid structure at the interface is changed by the adsorption. To highlight the change, the following quantity is introduced for the spatial distribution functions.

$$\Delta^{(2)} g_\gamma(\mathbf{r}) = g_\gamma\ (\mathbf{r};\ \text{surface with adsorbed molecule}) - g_\gamma\ (\mathbf{r};\ \text{bare surface}) \tag{10}$$

Figure 4(a) shows the changing in the distribution for the benzene system. The increased and decreased area are respectively colored in magenta and cyan, illustrating the iso-surface. As clearly seen, water molecules are excluded by the benzene from the surface, making $\Delta^{(2)} g_{\mathrm{O}}(\mathbf{r})$ and $\Delta^{(2)} g_{\mathrm{H}}(\mathbf{r})$ negative (cyan). At the same time the population of water molecules, just outside of these negative areas, are increased (colored in magenta). All of them are distributed in a hexagonal shape, covering the benzene molecule. It is interesting to note that the increasing of $g_{\mathrm{H}}(\mathbf{r})$ is limited just above the ring, presumably due to the negative charge on the carbon atoms. The distribution

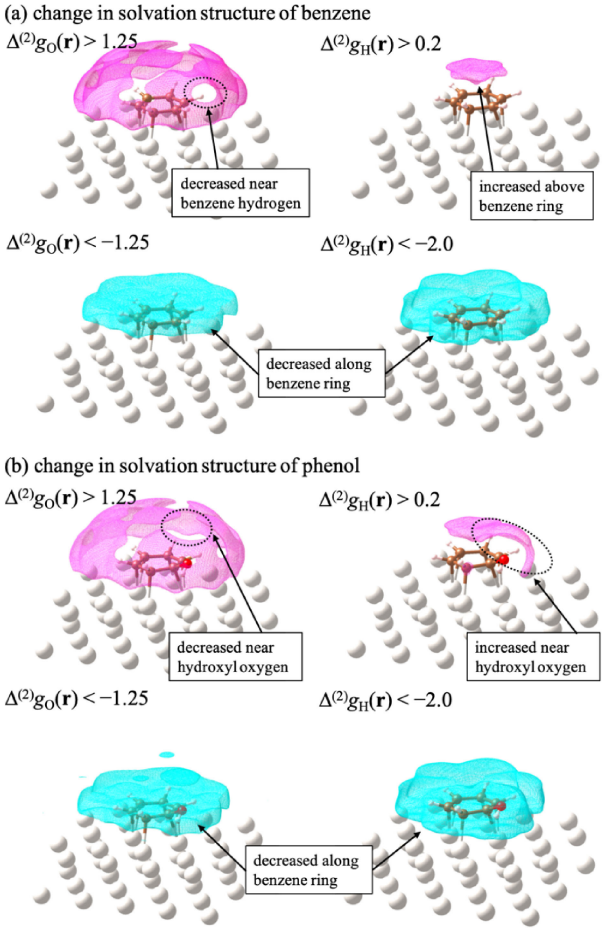

Figure 4. Difference in solvation structure between molecular adsorbed and bare Pt(111) surface for (a) benzene and (b) phenol for $\theta = 0.027$. Isovalues of $\Delta^{(2)}g_O(\mathbf{r})$ is 1.25 in both positive and negative differences, and those of $\Delta^{(2)}g_H(\mathbf{r})$ is 0.20 and 2.0 in positive and negative differences, respectively. This figure is produced by VESTA3 program.[47]

of water molecule outside of these regions remains essentially unchanged upon the absorption, meaning that the effect from the adsorption is relatively localized only in the vicinity of the adsorbent. The desolvated region of $g_H(\mathbf{r})$ has a larger thickness in the z-axis direction than that of $g_O(\mathbf{r})$, corresponding to the wider spatial distribution of $z = 2$ to 4 Å as shown in Figure 3.

The corresponding plot for phenol is shown in Figure 4(b). The shapes are deviated from hexagonal due to the introduction of the hydroxy group. A clear increment of $\Delta^{(2)}g_H(\mathbf{r})$ around the hydroxy group indicates the formation of hydrogen bonds between oxygen (phenol) and hydrogen (water). In the increment of $\Delta^{(2)}g_O(\mathbf{r})$, there are some low regions around the oxygen of the hydroxy group, which may be due to the electrostatic repulsion between oxygen (phenol) and oxygen (water).

Multiplying eq. (10) by the density of the solvent and integrating over the entire space gives an estimate of the number of water molecules. In the case of benzene adsorption, integrating the positive and negative regions respectively yield 7.5 and −13.5, corresponding to a decrease of 6.0 water in the balance. For phenol, integrating the positive and negative areas, respectively, yields 7.7 and −14.3, which means a decrease of 6.6 water molecules in the balance. The obtained number is close to the experimentally estimated number of water molecules, 6.5.[3]

In conclusion, we have computed free energy for the adsorption of aromatic molecules at the Pt(111)/water interface using 3D-RISM theory and DFT. Changes in solvation structure near the interface due to adsorption were also clarified. The free energy of desorption of water adsorbed on a surface is estimated more accurately than that with standard PCM method.

The authors thank Dr. Ryoichi Fukuda for fruitful discussion. This work was supported by JSPS KAKENHI and JST SPRING (Grant Numbers JP17H03009, JP20H05839 and JPMJSP2110). Theoretical computations were partly performed using Research Center for Computational Science, Okazaki, Japan (Project: 21-IMS-C021).

Supporting Information is available on https://doi.org/10.1246/cl.220215.

References

1 M. Saleheen, A. Heyden, *ACS Catal.* **2018**, *8*, 2188.
2 N. Singh, U. Sanyal, J. L. Fulton, O. Y. Gutiérrez, J. A. Lercher, C. T. Campbell, *ACS Catal.* **2019**, *9*, 6869.
3 N. Singh, C. T. Campbell, *ACS Catal.* **2019**, *9*, 8116.
4 J. Akinola, I. Barth, B. R. Goldsmith, N. Singh, *ACS Catal.* **2020**, *10*, 4929.
5 F. Lu, G. N. Salaita, L. Laguren-Davidson, D. A. Stern, E. Wellner, D. G. Frank, N. Batina, D. C. Zapien, N. Walton, A. T. Hubbard, *Langmuir* **1988**, *4*, 637.
6 J. O. Bockris, K. T. Jeng, *J. Electroanal. Chem.* **1992**, *330*, 541.
7 J. Akinola, C. T. Campbell, N. Singh, *J. Phys. Chem. C* **2021**, *125*, 24371.
8 P. Clabaut, B. Schweitzer, A. W. Götz, C. Michel, S. N. Steinmann, *J. Chem. Theory Comput.* **2020**, *16*, 6539.
9 G. Bramley, M.-T. Nguyen, V.-A. Glezakou, R. Rousseau, C.-K. Skylaris, *J. Chem. Theory Comput.* **2020**, *16*, 2703.
10 G. A. Bramley, M.-T. Nguyen, V.-A. Glezakou, R. Rousseau, C.-K. Skylaris, *J. Chem. Theory Comput.* **2022**, *18*, 1849.
11 S. A. Petrosyan, J.-F. Briere, D. Roundy, T. A. Arias, *Phys. Rev. B* **2007**, *75*, 205105.
12 K. Mathew, R. Sundararaman, K. Letchworth-Weaver, T. A. Arias, R. G. Hennig, *J. Chem. Phys.* **2014**, *140*, 084106.
13 S. N. Steinmann, P. Sautet, C. Michel, *Phys. Chem. Chem. Phys.* **2016**, *18*, 31850.
14 V. Shapovalov, T. N. Truong, A. Kovalenko, F. Hirata, *Chem. Phys. Lett.* **2000**, *320*, 186.
15 J. J. Howard, J. S. Perkyns, N. Choudhury, B. M. Pettitt, *J. Chem. Theory Comput.* **2008**, *4*, 1928.
16 A. Kovalenko, F. Hirata, *Chem. Phys. Lett.* **1998**, *290*, 237.
17 A. Kovalenko, F. Hirata, *J. Chem. Phys.* **1999**, *110*, 10095.
18 S. Nishihara, M. Otani, *Phys. Rev. B* **2017**, *96*, 115429.
19 K. Kasahara, H. Sato, *Chem. Lett.* **2018**, *47*, 311.
20 K. Iida, *J. Phys. Chem. C* **2022**, *126*, 7492.
21 S. Gautier, S. N. Steinmann, C. Michel, P. Fleurat-Lessard, P. Sautet, *Phys. Chem. Chem. Phys.* **2015**, *17*, 28921.
22 N. Chaudhary, A. Hensley, G. Collinge, Y. Wang, J.-S. McEwen, *J. Phys. Chem. C* **2020**, *124*, 356.

23 G. Kresse, J. Furthmüller, *Phys. Rev. B* **1996**, *54*, 11169.
24 G. Kresse, J. Furthmüller, *Comput. Mater. Sci.* **1996**, *6*, 15.
25 J. P. Perdew, K. Burke, M. Ernzerhof, *Phys. Rev. Lett.* **1996**, *77*, 3865.
26 P. E. Blöchl, *Phys. Rev. B* **1994**, *50*, 17953.
27 S. N. Steinmann, C. Corminboeuf, *J. Chem. Phys.* **2011**, *134*, 044117.
28 G. Makov, M. C. Payne, *Phys. Rev. B* **1995**, *51*, 4014.
29 H. J. Monkhorst, J. D. Pack, *Phys. Rev. B* **1976**, *13*, 5188.
30 A. V. Marenich, S. V. Jerome, C. J. Cramer, D. G. Truhlar, *J. Chem. Theory Comput.* **2012**, *8*, 527.
31 T. A. Manz, D. S. Sholl, *J. Chem. Theory Comput.* **2010**, *6*, 2455.
32 T. A. Manz, D. S. Sholl, *J. Chem. Theory Comput.* **2012**, *8*, 2844.
33 J. Z. Vilseck, J. Tirado-Rives, W. L. Jorgensen, *J. Chem. Theory Comput.* **2014**, *10*, 2802.
34 J. S. Perkyns, B. M. Pettitt, *Chem. Phys. Lett.* **1992**, *190*, 626.
35 A. K. Rappe, C. J. Casewit, K. S. Colwell, W. A. Goddard, III, W. M. Skiff, *J. Am. Chem. Soc.* **1992**, *114*, 10024.
36 H. Heinz, R. A. Vaia, B. L. Farmer, R. R. Naik, *J. Phys. Chem. C* **2008**, *112*, 17281.
37 C. T. Campbell, J. R. V. Sellers, *J. Am. Chem. Soc.* **2012**, *134*, 18109.
38 S. J. Carey, W. Zhao, Z. Mao, C. T. Campbell, *J. Phys. Chem. C* **2019**, *123*, 7627.
39 H. Ihm, H. M. Ajo, J. M. Gottfried, P. Bera, C. T. Campbell, *J. Phys. Chem. B* **2004**, *108*, 14627.
40 R. Parthasarathi, V. Subramanian, N. Sathyamurthy, *J. Phys. Chem. A* **2005**, *109*, 843.
41 A. Plugatyr, I. Nahtigal, I. M. Svishchev, *J. Chem. Phys.* **2006**, *124*, 024507.
42 O. Björneholm, M. H. Hansen, A. Hodgson, L.-M. Liu, D. T. Limmer, A. Michaelides, P. Pedevilla, J. Rossmeisl, H. Shen, G. Tocci, E. Tyrode, M.-M. Walz, J. Werner, H. Bluhm, *Chem. Rev.* **2016**, *116*, 7698.
43 S. Schnur, A. Groß, *New J. Phys.* **2009**, *11*, 125003.
44 L. Bellarosa, R. García-Muelas, G. Revilla-López, N. López, *ACS Cent. Sci.* **2016**, *2*, 109.
45 K. Iida, H. Sato, *J. Chem. Phys.* **2011**, *135*, 244702.
46 T. Ludwig, J. A. Gauthier, K. S. Brown, S. Ringe, J. K. Nørskov, K. Chan, *J. Phys. Chem. C* **2019**, *123*, 5999.
47 K. Momma, F. Izumi, *J. Appl. Crystallogr.* **2011**, *44*, 1272.

